Available online at www.sciencedirect.com
ScienceDirect
Journal of Sound and Vibration 317 (2008) 496–513
JOURNAL OF SOUND AND VIBRATION
www.elsevier.com/locate/jsvi

The actuated performance of multi-layer piezoelectric actuator in active vibration control of honeycomb sandwich panel

Yajun Luo, Shilin Xie, Xinong Zhang*

Department of Engineering Mechanics/MOE Key Laboratory for Strength and Vibration, School of Aerospace, Xi'an Jiaotong University, Xi'an 710049, PR China

Received 30 May 2007; received in revised form 16 March 2008; accepted 21 March 2008
Handling Editor: L.G. Tham
Available online 21 May 2008

Abstract

This paper discusses the use of the multi-layer piezoelectric actuator (MPA) in the active vibration control of the honeycomb sandwich panel (HSP). A literature overview of the available works is first presented. And the main motivation using the MPA in the AVC of HSP is discussed. Then, the honeycomb core is in advance treated as an orthotropic plate. The governing equations of the system are derived by the Hamilton principle on the basis of both displacement and transverse tress assumptions. The formulations of the actuation force/moment are obtained and indicate that the actuation force/moment are two four-order polynomial function of the piezoelectric layers number. Finally, active control experiments of a cantilever honeycomb sandwich panel (CHSP) are performed using the MPA. The control law of proportional velocity feedback is adopted in the experiments. These experiments include the resonant vibration control and the sinusoidal swept of the control system at the case of different piezoelectric layers number. The results show that the MPA can effectively control the vibration of the high damping HSP, and the control performance per voltage by the proposed actuator can be improved significantly through increasing the piezoelectric patch number. Consequently, the MPA exhibits better actuation capability than that with only single layer.

1. Introduction

The honeycomb sandwich structure was widely used in the aeronautic and astronautic engineering due to its advantages such as large specific stiffness and specific strength [1]. A practical example is the apparatus cabin of launch vehicle, where a lot of honeycomb sandwich panels (HSP) are utilized to install some important flight control instruments, for example, the telemetric devices, the gyroscope and so on. The external disturbances generally excite these HSPs into resonances, which influence seriously the accuracy and reliability of the control devices placed on them. In order to ensure the safety of flight, the vibration of the HSP must be attenuated effectively. The HSP, as typical composite structures, are inherently more difficult to model than their metallic counterparts, not to mention their potential heterogeneities and the differences in dynamic

*Corresponding author. Tel.: +86 29 82668757x802; fax: +86 29 82669044.
E-mail addresses: luoyajun@mail.xjtu.edu.cn (Y. Luo), xnzhang@mail.xjtu.edu.cn (X. Zhang).

0022-460X/$ - see front matter © 2008 Elsevier Ltd. All rights reserved.
doi:10.1016/j.jsv.2008.03.047

behavior between supposedly identical samples. Moreover, the high level of structural damping exhibited by them adds to the difficulty of dynamic analysis. So there are only several reports about their active control and these literatures as followings: the active vibration control experiments of certain HSP for mounting apparatuses using a single PZT patch are studied by Luo et al. [2]. The active control experiments for acoustic radiation reduction of the HSP adopting PVDF and PZT patches are worked by Petitjean et al. [3].

In present, the investigation of the piezoceramic material actuators in the structural control fields have been reported richly, example for the journal articles [4–6]. Unfortunately, in order to provide sufficient actuated forces, most of them are limited to either a number of discrete rectangular patches or a single thin sheet. One of the major drawbacks of the discrete patches requires careful management of higher modes and as a result, the control schemes become highly involved and difficult to implement. On the other hand, single sheet form is the modal phase cancellation, which severely restricts the control capability for higher vibration modes of the structure. A single piezoelectric patch, whether one-sided, or in the bimorph form, has a fairly low voltage-strain sensitivity and hence cannot generate a large control force. One way of increasing the actuator sensitivity is to use very high input voltages, but this can lead to problems of patch burning as well as additional safety requirements while working with high voltages. Moreover, the high voltages are not usually supplied by work environment. Considered above causes, Zhang et al. [7] and Joshi [8] refer to the multi-layer piezoelectric actuator (MPA). The MPA is a simple way that uses a larger number of layers at the same point, one below the other in the thickness direction, and drives the same input voltage for its every layer. Zhang provide the active control experiments approach which the MPA bonds on the surface of the structure. Joshi investigates the voltage moment sensitivity of the MPA, as an actuator for vibration control, embedded into the surface of the thin-walled beam-type structures. It is indicated that the MPA can increase the force output for the low input voltage and littler varies the mass, stiffness and strength of the structure controlled by them.

Consequently, it is approached to control the vibration of the HSP using the MPA in this paper. Because the thickness of the MPA is usually large than that of the face sheet of the HSP, it will combine with the HSP hard if it is embedded into the surface of the HSP. In order to achieve the apply of the MPA, it should be bonded on the surface of the HSP. This way is just adopted in this paper. However, the HSP attached to the MPA is a complicated laminated structure. There have been many articles addressing the modeling of laminated structures so far [9–15]. Especially, Carrera [14] gave a full review and summarization on well-known zig-zag theories for multilayered plates and shells, and built a uniform dynamic formulation of piezoelectric laminated structures based on Makumina's zig-zag theory [15]. This theory is considerably exhaustive and can commonly bring forth a problem solution of high accuracy. However, it needs to be pointed out that the actuator is not bonded on the whole surface of honeycomb structure as those discussed in the above-mentioned literatures but bonded on the local surface of structure at the present case. It thus makes the influences of the piezoelectric actuator on inertia and stiffness properties of the full structure weak. This means that the honeycomb structure dominates the dynamic characteristics of the full structure. A recent study by Yu and Cleghorn indicated only Reddy's third-order plate theory is adequate for analyzing the vibration of HSP with respect to the classical plate theory and Mindlin's improved plate theory [16]. Considering this point and the feature of problem at hand, a revised Reddy's third-order plate theory is developed through introducing the Heaviside function into the original Reddy's third-order plate theory [17] for modeling the system in the present study.

To the single layer piezoelectric actuator, the applications in active control system have been reported early [18,19]. The influences of some important parameters, such as the bonded displacement on the structure and the size, on the effect of the vibration control have been widely studied in recent years [20–22]. Based on the definition of the MPA in this paper, it is a sort of strain-type actuator all the same and its actuated manner is same to the single layer piezoelectric actuator. The only difference is the piezoelectric layer number. Consequently, our main intention is to compare the actuated performance of the MPA with different piezoelectric layer number. The other parameters will not be discussed in detail here.

The paper is organized as follows: in Section 2, based on the revised Reddy's third-order plate theory, the electromechanical coupling equation of the system is derived using Hamilton principle. In Section 3, the actuation force and moment exerted by the MPA are examined in terms of the number of piezoelectric patches used. In Section 4, the actuation ability of the MPA is evaluated and compared at the case of different

piezoelectric patch number through active control experiments for a cantilever honeycomb sandwich panel (CHSP). The concluding remarks are given in Section 5.

2. Governing equations

The control system considered in this study is shown in Fig. 1. The controlled structure is an HSP made up of two thin faceplates (i.e., the top and bottom faceplates) and a thick honeycomb core. The top and bottom faceplates are isotropic and with the same geometric and material parameters. The honeycomb core is composed of hexagon honeycomb elements and thereby possesses orthotropic elasticity property. A MPA is bonded on the top faceplate to actively control the vibrations of HSP. Fig. 2 shows cross section view of the control system, where the MPA consists of N identical piezoelectric patches. All piezoelectric patches are polarized along the normal direction and bonded together through the surfaces with the same polarity to fabricate the MPA. Each piezoelectric patch in the MPA is orientated specially so as to possess the identical piezoelectric stress coefficients. Besides, each piezoelectric patch is applied with identical control voltage. In this way, one can expect that the MPA generates greater actuation force or moment on controlled structure through in-plane deformations of all piezoelectric patches in terms of inverse piezoelectric effect than a single piezoelectric patch actuator. Note that working principle of the MPA is different from that of traditional piezoelectric stack actuator, which exerts control force through out-of-plane deformation.

2.1. Assumptions

It is shown from Fig. 2 that the HSP and the MPA (including piezoelectric patches and adhesive layers) constitute a complicated laminated structure. The coordinate system X–Y–Z shown in Fig. 1 is used to

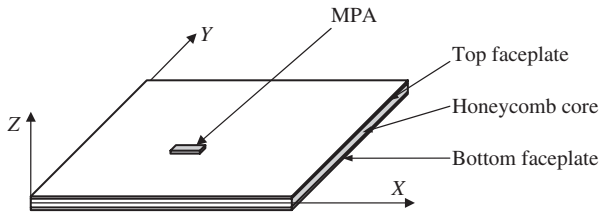

Fig. 1. The control system considered in the study.

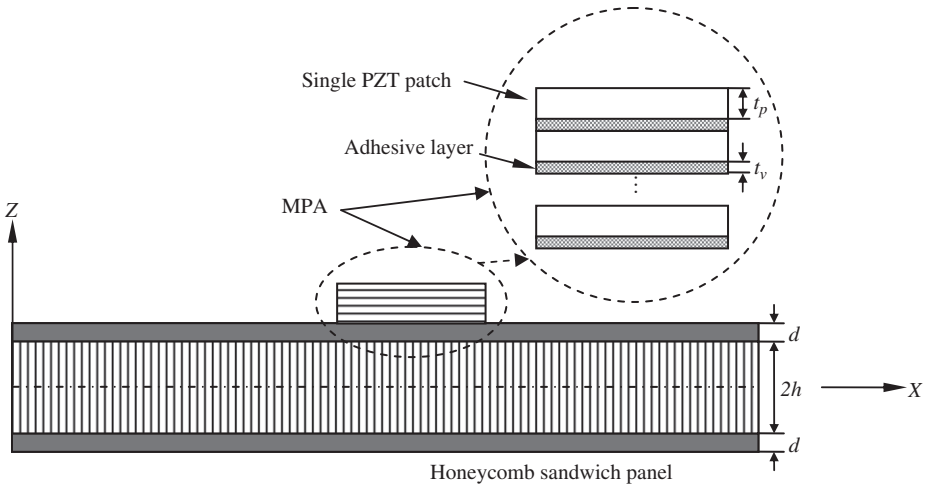

Fig. 2. The cross section view of the control system.

describe the motion of the laminated structure. The X–Y plane coincides with the mid-plane of HSP. In order to facilitate derivation of governing equation of such a laminated structure, the following assumptions are made:

(1) Both the piezoelectric patch and adhesive layer are isotropic.
(2) Three material principal directions of the honeycomb core are identical with the X, Y and Z directions, respectively.
(3) The honeycomb core is treated as an orthotropic plate with the same mass and geometric dimensions.
(4) The neutral-plane of the laminated structure coincides with mid-plane of the HSP.
(5) The transverse strain of the laminated structure equals zero (i.e. $\varepsilon_z = 0$).
(6) The transverse shearing strains of the laminated structure cannot be neglected but equal zero at the top and bottom surfaces of laminated structure.

According to Reddy third-order shear theory [17], the displacement functions of the laminated structure satisfying the above assumptions can be given as

$$u(x,y,z,t) = z\varphi_x - \frac{z^3}{3[h+d+H(x,y,z)N(t_p+t_v)]^2}\left(\varphi_x + \frac{\partial w}{\partial x}\right), \tag{1a}$$

$$v(x,y,z,t) = z\varphi_y - \frac{z^3}{3[h+d+H(x,y,z)N(t_p+t_v)]^2}\left(\varphi_y + \frac{\partial w}{\partial y}\right), \tag{1b}$$

$$w = w(x,y,t), \tag{1c}$$

where u, v and w are the displacement in the X, Y and Z directions, respectively, φ_x and φ_y are the rotation angel about the Y- and X-axis, respectively, h is the half-thickness of the honeycomb core, d is the thickness of the faceplates, t_p and t_v are the thickness of single piezoelectric patch and single adhesive layer, respectively, t is the time argument, $H(x, y, z)$ is the third-order Heaviside function associated with location of the MPA

$$H(x,y,z) = [H_0(x-x_1) - H_0(x-x_2)][H_0(y-y_1) - H_0(y-y_2)]H_0(z), \tag{2}$$

where H_0 represents the unit step function ($H_0 = 1$ if $x \geqslant 0$ and $H_0 = 0$ otherwise), x_1 and x_2 are the X-coordinates of boundaries of the actuator, respectively, and y_1 and y_2 are the Y-coordinates of boundaries of the actuator, respectively.

2.2. Constitutive equations

The geometric equation of the laminated structure is

$$\{\,\varepsilon_x \quad \varepsilon_y \quad \gamma_{xz} \quad \gamma_{yz} \quad \gamma_{xy}\,\}^{\mathrm{T}} = \left[\frac{\partial u}{\partial x} \quad \frac{\partial v}{\partial y} \quad \frac{\partial u}{\partial z}+\frac{\partial w}{\partial x} \quad \frac{\partial v}{\partial z}+\frac{\partial w}{\partial y} \quad \frac{\partial u}{\partial y}+\frac{\partial v}{\partial x}\right]^{\mathrm{T}}, \tag{3}$$

where ε_x and ε_y are the linear strain in the X and Y direction, respectively, γ_{xz}, γ_{yz} and γ_{xy} are the shearing strain in the X–Z, Y–Z and X–Y plane, respectively, and the symbol T denotes the transpose of a matrix or vector.

Based on the above assumptions, the constitutive equations of both HSP and adhesive layer can be written as

$$\begin{Bmatrix} \sigma_x^{\mathrm{syb}} \\ \sigma_y^{\mathrm{syb}} \\ \tau_{xz}^{\mathrm{syb}} \\ \tau_{yz}^{\mathrm{syb}} \\ \tau_{xy}^{\mathrm{syb}} \end{Bmatrix} = \begin{bmatrix} c_{11}^{\mathrm{syb}} & c_{12}^{\mathrm{syb}} & & & \\ c_{12}^{\mathrm{syb}} & c_{22}^{\mathrm{syb}} & & & \\ & & c_{44}^{\mathrm{syb}} & & \\ & & & c_{55}^{\mathrm{syb}} & \\ & & & & c_{66}^{\mathrm{syb}} \end{bmatrix} \begin{Bmatrix} \varepsilon_x^{\mathrm{syb}} \\ \varepsilon_y^{\mathrm{syb}} \\ \gamma_{xz}^{\mathrm{syb}} \\ \gamma_{yz}^{\mathrm{syb}} \\ \gamma_{xy}^{\mathrm{syb}} \end{Bmatrix}, \tag{4}$$

where the symbol c represents elasticity coefficient, the superscript *syb* indicates different structures. Eq. (4) describes the faceplate for syb = '*f*', the honeycomb core for syb = '*c*', and the adhesive layer for syb = '*v*'.

The constitutive equation of the piezoelectric patch can be expressed as

$$\begin{Bmatrix} \sigma_x^p \\ \sigma_y^p \\ \tau_{xz}^p \\ \tau_{yz}^p \\ \tau_{xy}^p \end{Bmatrix} = \begin{bmatrix} c_{11}^p & c_{12}^p & & & \\ c_{12}^p & c_{22}^p & & & \\ & & \dfrac{c_{11}^p - c_{12}^p}{2} & & \\ & & & \dfrac{c_{11}^p - c_{12}^p}{2} & \\ & & & & \dfrac{c_{11}^p - c_{12}^p}{2} \end{bmatrix} \begin{Bmatrix} \varepsilon_x^p \\ \varepsilon_y^p \\ \gamma_{xz}^p \\ \gamma_{yz}^p \\ \gamma_{xy}^p \end{Bmatrix} - \begin{Bmatrix} e_{31} \\ e_{32} \\ 0 \\ 0 \\ 0 \end{Bmatrix} E_3, \tag{5}$$

where the superscript p represents the piezoelectric patch, e_{31} and e_{32} are the piezoelectric stress coefficient in the X and Y directions, respectively, and E_3 is the electric field applied on each piezoelectric patch in the Z direction. Here, it should be noted that the elasticity and piezoelectric coefficients appeared in Eqs. (4) and (5) do not correspond to those in a 3D constitutive equation but the modified ones derived from zero-normal stress assumption [23].

2.3. Governing equations

The Hamilton equation of the laminated structure shown in Fig. 2 can be expressed as

$$\delta \int_{t_1}^{t_2} (T - U + A)\mathrm{d}t = 0, \tag{6}$$

$$T = T^f + T^c + T^p + T^v, \tag{7}$$

$$U = U^f + U^c + U^p + U^v, \tag{8}$$

where δ is the variational operator, T and U are the total kinetic energy and total potential energy of the laminated structure, respectively, A is the total work provided by external loading, T^f, T^c, T^p and T^v are the kinetic energy of two faceplates, honeycomb core, all piezoelectric patches and all adhesive layers, respectively, and U^f, U^c, U^p and U^v are the potential energy of two faceplates, honeycomb core, all piezoelectric patches and all adhesive layers, respectively.

From Eq. (1), the components of the total kinetic energy of the laminated structure is derived as

$$\begin{aligned} \{T^f\, T^c\, T^p\, T^v\}^{\mathrm{T}} = \frac{1}{2}\int_0^b \int_0^a [&\{I_0^f I_0^c HI_0^p HI_0^v\}^{\mathrm{T}} \dot{w}^2 + \{I_1^f I_1^c HI_1^p HI_1^v\}^{\mathrm{T}} (\dot{\varphi}_x^2 + \dot{\varphi}_y^2) \\ &- \{I_2^f I_2^c HI_2^p HI_2^v\}^{\mathrm{T}} (\dot{\varphi}_x^2 + \dot{\varphi}_y^2 + \dot{\varphi}_x \dot{\varphi}_{,x} + \dot{\varphi}_y \dot{\varphi}_{,y}) + \{I_3^f I_3^c HI_3^p HI_3^v\}^{\mathrm{T}} \\ &\times (\dot{\varphi}_x^2 + \dot{\varphi}_y^2 + 2\dot{\varphi}_x \dot{w}_{,x} + 2\dot{\varphi}_y \dot{w}_{,y} + \dot{w}_{,x}^2 + \dot{w}_{,y}^2)]\mathrm{d}x\, \mathrm{d}y, \end{aligned} \tag{9}$$

where a and b are the length of the HSP in the X and Y directions, respectively, the subscript "," represents partial differential operation, I_i^f, I_i^c, I_i^p and I_i^v ($i = 0,1,2,3$) represent the generalized inertia of two faceplates, honeycomb core, all piezoelectric patches and all adhesive layers, respectively, and

$$I_i^f = \tilde{A}_i \tilde{B}_i \left[\int_{-h-d}^{-h} \rho^f z^{2i}\, \mathrm{d}z + \int_h^{h+d} \rho^f z^{2i}\, \mathrm{d}z \right], \tag{10a}$$

$$I_i^c = \tilde{A}_i \tilde{B}_i \int_{-h}^{h} \rho^c z^{2i}\, \mathrm{d}z, \tag{10b}$$

$$I_i^p = \tilde{A}_i \tilde{B}_i \sum_{j=1}^{N} \int_{h+d+jt_v+(j-1)t_p}^{h+d+jt_v+jt_p} \rho^p z^{2i}\,\mathrm{d}z, \tag{10c}$$

$$I_i^v = \tilde{A}_i \tilde{B}_i \sum_{j=1}^{N} \int_{h+d+(j-1)t_v+(j-1)t_p}^{h+d+jt_v+(j-1)t_p} \rho^v z^{2i}\,\mathrm{d}z, \tag{10d}$$

where ρ^f, ρ^c, ρ^p, and ρ^v are the mass density of faceplate, honeycomb core, piezoelectric patch and adhesive layer, respectively, and the coefficients $\tilde{A}_i$ and $\tilde{B}_i$ ($i = 0,1,2,3$) satisfy

$$\tilde{A}_i = \begin{cases} 1 & \text{for} \quad i = 0,1, \\ 2/3 & \text{for} \quad i = 2, \\ 1/9 & \text{for} \quad i = 3, \end{cases}$$

$$\tilde{B}_i = \begin{cases} 1 & \text{for} \quad i = 0,1 \\ [h + d + H(x,y,z)N(t_p + t_v)]^{-2(i-1)} & \text{for} \quad i = 2,3 \end{cases}$$

Neglecting the electrical potential energy in piezoelectric patches resulting from electric displacement, and utilizing Eqs. (1)–(5) we can obtain the components of the total potential energy of the laminated structure as

$$\begin{aligned} \{U^f\ U^c\ U^p\ U^v\}^{\mathrm{T}} = \frac{1}{2}\int_0^b \int_0^a [&\mathbf{M}_x\varphi_{x,x} + \mathbf{M}_y\varphi_{y,y} + \mathbf{M}_{xy}(\varphi_{x,y} + \varphi_{y,x}) - \mathbf{R}_x(\varphi_{x,x} + w_{,xx}) \\ &- \mathbf{R}_y(\varphi_{y,y} + w_{,yy}) - \mathbf{R}_{xy}(\varphi_{x,y} + \varphi_{y,x} + 2w_{,xy}) + (\mathbf{Q}_{yz} - \mathbf{T}_{yz})(\varphi_y + w_{,y}) \\ &+ (\mathbf{Q}_{xz} - \mathbf{T}_{xz})(\varphi_x + w_{,x})]\mathrm{d}x\,\mathrm{d}y, \end{aligned} \tag{11}$$

$$\begin{aligned} \mathbf{M}_x &= \{\, M_x^f \quad M_x^c \quad HM_x^p \quad HM_x^v \,\}^{\mathrm{T}}, \\ \mathbf{M}_y &= \{\, M_y^f \quad M_y^c \quad HM_y^p \quad HM_y^v \,\}^{\mathrm{T}}, \\ \mathbf{M}_{xy} &= \{\, M_{xy}^f \quad M_{xy}^c \quad HM_{xy}^p \quad HM_{xy}^v \,\}^{\mathrm{T}}, \\ \mathbf{R}_x &= \{\, R_x^f \quad R_x^c \quad HR_x^p \quad HR_x^v \,\}^{\mathrm{T}}, \\ \mathbf{R}_y &= \{\, R_y^f \quad R_y^c \quad HR_y^p \quad HR_y^v \,\}^{\mathrm{T}}, \\ \mathbf{R}_{xy} &= \{\, R_{xy}^f \quad R_{xy}^c \quad HR_{xy}^p \quad HR_{xy}^v \,\}^{\mathrm{T}}, \\ \mathbf{Q}_{xz} &= \{\, Q_{xz}^f \quad Q_{xz}^c \quad HQ_{xz}^p \quad HQ_{xz}^v \,\}^{\mathrm{T}}, \\ \mathbf{Q}_{yz} &= \{\, Q_{yz}^f \quad Q_{yz}^c \quad HQ_{yz}^p \quad HQ_{yz}^v \,\}^{\mathrm{T}}, \\ \mathbf{T}_{xz} &= \{\, T_{xz}^f \quad T_{xz}^c \quad HT_{xz}^p \quad HT_{xz}^v \,\}^{\mathrm{T}}, \\ \mathbf{T}_{yz} &= \{\, T_{yz}^f \quad T_{yz}^c \quad HT_{yz}^p \quad HT_{yz}^v \,\}^{\mathrm{T}}, \end{aligned}$$

where $\mathbf{M}_x$ and $\mathbf{M}_y$ are the generalized bending moment vectors, $\mathbf{M}_{xy}$ is the generalized torsion moment vector, $\mathbf{R}_x$ and $\mathbf{R}_y$ are the generalized third-order bending moment vectors, $\mathbf{R}_{xy}$ is the generalized third-order torsion moment vector, $\mathbf{Q}_{xz}$ and $\mathbf{Q}_{yz}$ are the generalized transverse shear force vectors, $\mathbf{T}_{xz}$ and $\mathbf{T}_{yz}$ are the generalized third-order transverse shear force vectors. The detailed expressions for all components of each generalized internal force/moment vector are shown in Appendix A.

Assuming the laminated structure is only subjected to transverse distributed force $q(x,y,t)$, then the total work provided by external force is

$$A = \int_0^b \int_0^a q(x,y,t)w \,\mathrm{d}x\,\mathrm{d}y + \int_0^b [\mathbf{M}_x^{bc}\varphi_x + \mathbf{M}_{xy}^{bc}\varphi_y + \mathbf{Q}_{xz}^{bc}w - \mathbf{R}_x^{bc}(\varphi_x + w_{,x}) - \mathbf{R}_{xy}^{bc}(\varphi_y + w_{,y})]|_0^a \,\mathrm{d}y + \int_0^a [\mathbf{M}_{xy}^{bc}\varphi_x + \mathbf{M}_y^{bc}\varphi_y + \mathbf{Q}_{yz}^{bc}w - \mathbf{R}_{xy}^{bc}(\varphi_x + w_{,x}) - \mathbf{R}_y^{bc}(\varphi_y + w_{,y})]|_0^b \,\mathrm{d}x \tag{12}$$

where the first term of right-hand side of equation represents the work provided by the transverse distributed force, and the second and third terms represent that by boundary conditions of the structure. Note that the actuator is free at four sides for the present case, hence, only the boundary conditions of HSP need to be considered in the calculations.

Substituting Eqs. (9), (11) and (12) into Eq. (6), and then performing the variations with respect to the displacement function φ_x, φ_y and w, respectively, yields the governing equations of the laminated structure as follows:

$$[K_1^h + HK_1^m]\varphi_{x,xx} + [K_2^h + HK_2^m]\varphi_{x,yy} + [K_3^h + HK_3^m]\varphi_{y,xy} + [K_4^h + HK_4^m]w_{,xxx} + [K_5^h + HK_5^m]w_{,xyy} + K_6^h(\varphi_x + w_{,x}) + (I_1 + I_3 - I_2)\ddot{\varphi}_x + (I_3 - I_2/2)\ddot{w}_{,x} = (A_5^p - D_5^p)H_{,x}e_{31}E_3, \tag{13a}$$

$$[L_1^h + HL_1^m]\varphi_{x,xy} + [L_2^h + HL_2^m]\varphi_{y,xx} + [L_3^h + HL_3^m]w_{,xxy} + [L_4^h + HL_4^m]\varphi_{y,yy} + [L_5^h + HL_5^m]w_{,yyy} + L_6^h(\varphi_y + w_{,y}) + (I_1 + I_3 - I_2)\ddot{\varphi}_y + (I_3 - I_2/2)\ddot{w}_{,y} = (B_5^p - E_5^p)H_{,y}e_{32}E_3, \tag{13b}$$

$$[P_1^h + HP_1^m]\varphi_{x,xxx} + [P_2^h + HP_2^m]\varphi_{y,yyy} + [P_3^h + HP_3^m]\varphi_{y,xxy} + [P_4^h + HP_4^m]\varphi_{x,xyy} + [P_5^h + HP_5^m]w_{,xxxx} + [P_6^h + HP_6^m]w_{,xxyy} + [P_7^h + HP_7^m]w_{,yyyy} + P_8^h(\varphi_{x,x} + w_{,xx}) + P_9^h(\varphi_{y,y} + w_{,yy}) + I_0\ddot{w} + (I_2/2 - I_3)(\ddot{\varphi}_{x,x} + \ddot{\varphi}_{y,y}) - I_3(\ddot{w}_{,xx} + \ddot{w}_{,yy}) = D_5^p H_{,xx}e_{31}E_3 + E_5^p H_{,yy}e_{32}E_3 + q(x,y,t) \tag{13c}$$

where the superscripts h and m represent the HSP and the MPA, respectively, K_i^h, L_i^h $(i = 1,\ldots,6)$ and P_j^h $(j = 1,\ldots,9)$ are the coefficients associated with the generalized internal forces/moments in the HSP, K_i^m, L_i^m $(i = 1,\ldots,6)$ and P_j^m $(j = 1,\ldots,9)$ are the coefficients associated with the generalized internal forces/moments in the MPA, A_5^p, B_5^p, D_5^p and E_5^p are the coefficients associated with generalized actuation force generated by all piezoelectric patches in terms of inverse piezoelectric effect, I_k $(k = 0,\ldots,3)$ are the generalized inertias of the laminated structure and defined as $I_k = I_k^f + I_k^c + I_k^p + I_k^v$ $(k = 0,\ldots,3)$. The detailed expressions of the above coefficients are also given in Appendix A. All together, the boundary conditions in explicit form of the laminated structure can be obtained as shown in Appendix B.

3. Analysis of actuation forces of MPA

The solution of the governing equations is not easy for including third-order Heaviside functions, only the actuation forces by MPA are analyzed here. It is assumed that the electric field E_3 distributes uniformly along the Z direction, thus we have

$$E_3 = \frac{V_p}{t_p}, \tag{14}$$

where V_p is the control voltage applied to single piezoelectric patch. The terms containing the electric field variable E_3 on the right-hand side of Eq. (13) represent the actuation forces exerted by the MPA. In order to evaluate the actuating capability of the MPA, define the actuation forces/moments over unit area per control voltage respectively as

$$M_x^m = (A_5^p - D_5^p)\frac{e_{31}}{t_p} = \frac{e_{31}}{t_p}\sum_{k=1}^{N}\int_{h+d+kt_v+(k-1)t_p}^{h+d+kt_v+kt_p} \frac{z^3 - 3[h+d+HN(t_p+t_v)]^2 z}{3[h+d+HN(t_p+t_v)]^2}\,\mathrm{d}z, \tag{15a}$$

$$M_y^m = (B_5^p - E_5^p)\frac{e_{32}}{t_p} = \frac{e_{32}}{t_p}\sum_{k=1}^{N}\int_{h+d+kt_v+(k-1)t_p}^{h+d+kt_v+kt_p} \frac{z^3 - 3[h+d+HN(t_p+t_v)]^2 z}{3[h+d+HN(t_p+t_v)]^2}\,\mathrm{d}z, \tag{15b}$$

$$F_x^m = \frac{D_5^p e_{31}}{t_p} = \frac{e_{31}}{3[h+d+HN(t_p+t_v)]^2 t_p}\sum_{k=1}^{N}\int_{h+d+kt_v+(k-1)t_p}^{h+d+kt_v+kt_p} z^3\,\mathrm{d}z, \tag{15c}$$

$$F_y^m = \frac{E_5^p e_{32}}{t_p} = \frac{e_{32}}{3[h+d+HN(t_p+t_v)]^2 t_p}\sum_{k=1}^{N}\int_{h+d+kt_v+(k-1)t_p}^{h+d+kt_v+kt_p} z^3\,\mathrm{d}z, \tag{15d}$$

Table 1
The physical parameters of the laminated structure used to analyze actuation force produced by the MPA

e_{31} (C/m^2)	e_{32} (C/m^2)	t_p (mm)	t_v (mm)	h (mm)	d (mm)
16.1	16.1	1.0	0.1	4.8	0.3

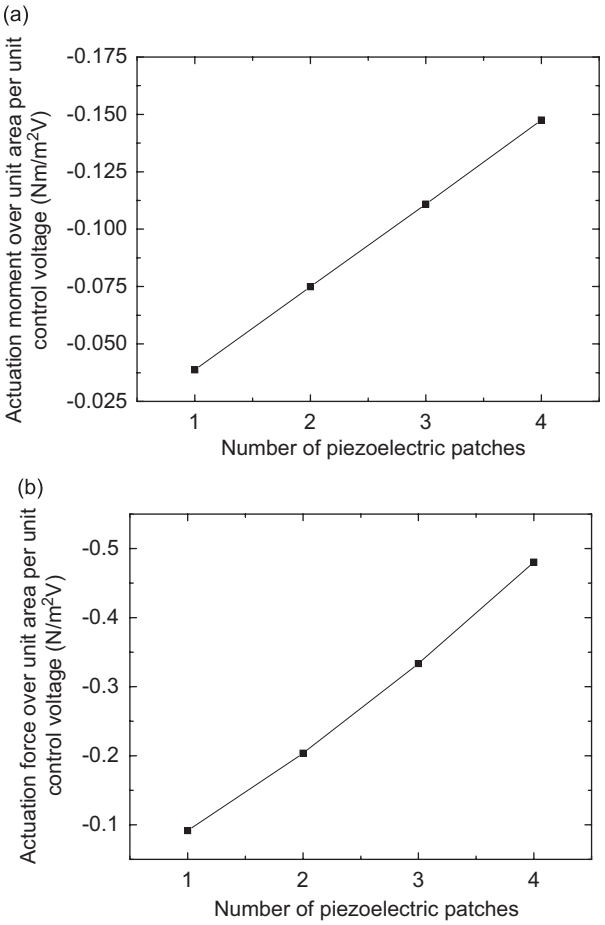

Fig. 3. The effects of the number of piezoelectric patches on actuation moment and actuation force over unit area per control voltage generated by the MPA: (a) actuation moment over unit area per control voltage; and (b) actuation force over unit area per control voltage.

where M_x^m and M_y^m are the actuation moment of the MPA in the X–Z and Y–Z planes, respectively, and F_x^m and F_y^m are the actuation force of the MPA in the X and Y directions, respectively. Note that, for clarity, the partial differentials of third-order Heaviside function $H(x, y, z)$ (including $H_{,x}$, $H_{,y}$, $H_{,xx}$ and $H_{,yy}$) are all not contained in the above definitions because they are relevant to the attached location of the actuator. It means that the actuation force/moments defined in Eqs. (15a), (15b), (15c) and (15d) are only in order to descript the actuated capability of MPA and not the real parameters.

In order to examine the effects of the number of piezoelectric patches (N) on the actuation force/moment over unit area per control voltage, a laminated structure with nominal physical parameters given in Table 1 is considered. From Table 1 it is shown that $e_{31} = e_{32}$, thus, only M_x^m and F_x^m need to be considered. Integrating Eqs. (15a) and (15c), respectively, one can obtain

$$M_x^m = \frac{e_{31}}{12(h+d)^2}\{(t_p+t_v)^3N^4 + 2(t_p+t_v)^2(t_v+2h+2d)N^3 + (t_p+t_v)[t_v(t_v-t_p) + 6(h+d)(h+d+t_v)]N^2 + [2(h+d)^2(2h+2d-6+3t_v) + 2t_v(h+d)(t_v-t_p) - t_v^2t_p]N\}, \quad (16)$$

$$F_x^m = \frac{-e_{31}}{12(h+d)^2}\{(t_p+t_v)^3N^4 + 2(t_p+t_v)^2(2h+2t_vd)N^3 + (t_p+t_v)[t_v(t_v-t_p) + 6(h+d)(h+d+t_v)]N^2 + (2h+2d+t_v)[2(h+d)(h+d+t_v) - t_vt_p]N\}. \quad (17)$$

It is shown form Eqs. (16) and (17) that both actuation moment and actuation force over unit area per control voltage generated by the MPA are the four-order polynomial functions of the number of used piezoelectric patches.

Figs. 3(a) and (b) show the effects of the number of piezoelectric patches (ranging from 1 to 4) on the magnitudes of actuation moment M_x^m and actuation force F_x^m, respectively, where the other physical parameters of laminated structure take the nominal values. It can be observed that, as expected, both the magnitudes of actuation moment M_x^m and the actuation force F_x^m over unit area per control voltage increase obviously as the number of piezoelectric patches increases. However, the relations are approximately linear between M_x^m/F_x^m and N. It can be indicated that the high-order terms of N have little effect to the amplitude of the actuation force/moments. Comparing the case of $N = 1$ with the case of $N = 4$, it is shown that the approximate 3.81 and 5.24 times improvement in magnitude are obtained for the actuation moment M_x^m and the actuation force F_x^m, respectively. It means that the actuating capability of the actuator can be enhanced significantly through using the more number of piezoelectric patches.

4. Active control experiments

In order to evaluate fully the actuation ability of the MPA, the active control experiment of a cantilever honeycomb sandwich panel (CHSP) is performed in this section.

4.1. Experimental setup

The vibration of the CHSP whose both honeycomb core and two faceplates are made up of aluminous metal will be controlled in the present experiments. The conformation of the controlled structural and the actuator is shown by Fig. 1 or Fig. 2. The CHSP is 500 mm long, 400 mm wide and 20 mm thick. A short edge of the HSP is clamped vertically by two thick armor plates which are fixed at the test stand. Each layer of the MPA is PZT patch whose sizes are 40 mm × 20 mm × 1 mm. The MPA with four layer PZT patches is considered in the experiments, and the way of applied voltage of the MPA is shown by Fig. 4. In order to provide the uniform

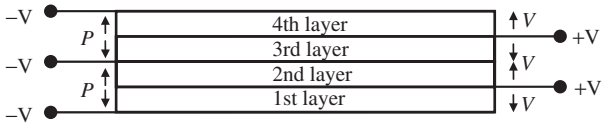

Fig. 4. The cross section view of the MPA.

actuated force, the same voltage V will be applied across each surfaces of all four patches along their polarization axes P, as shown in Fig. 4. Note that, for assurance insulation in MPA, all adjacent surfaces of the PZT patches will be applied a same polarity voltage. Finally, the 1st layer will attach to the surface of the CHSP.

In this paper, the first three eigenmodes will be considered in the vibration control. In order to obtain a high control performance, the strain-type actuator MPA should be attached on the area with great strain. Generally, the location with great gradient variation of the mode deformation is often selected. For choosing a suitable attached position, a modal test is executed. The CHSP is meshed by 10×8 elements and then the hammer excitation method is adopted. As shown in Fig. 5, the mode shape of the first three eigenmodes and the responding attached area of the MPA are illustrated. In Fig. 5, the bottle side is fixed and the deeper color denotes the smaller amplitude of mode deformation. Based on the mode shapes results, the attached area of the MPA is chosen as shown by the white rectangle.

The layout of the feedback vibration control experiments of the CHSP is shown by Fig. 6. The signals are measured and analyzed by the PULSE system (B&K), and the excited signs are generated from it. The control action of the feedback controller is generated by the MPA. The design and realization of the feedback control law is done by the dSPACE DS1103 system. In experiments, the simulated flow diagram design by MATLAB\Simulink is compiled, and then the ControlDesk software of dSPACE system will call these compiled files and designs the control platform to perform the experiments. Both PULSE and dSPACE system can be interacted with ones by personal computers. The other apparatuses include a Power Amplifier (Power AMP, model HEAS-50 from NAAU), a electromagnetic shaker (XJTU) whose excited point located the point E, a Charge Amplifier (Charge AMP, model BK2635 from B&K), an acceleration transducer

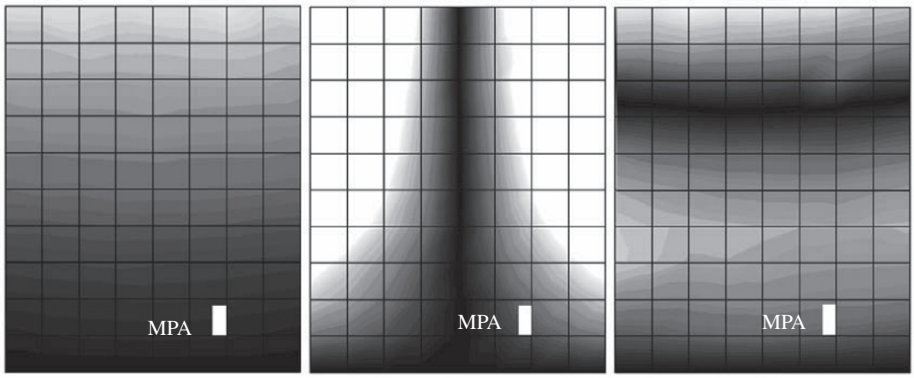

Fig. 5. The mode shapes and the position of MPA.

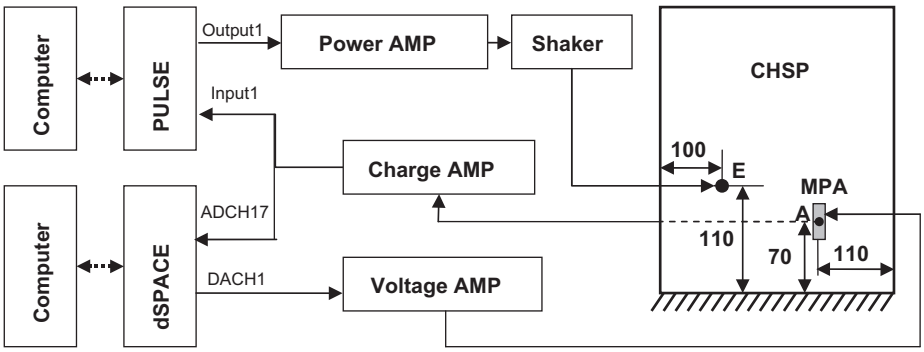

Fig. 6. The layout of the feedback vibration control experiments of the CHSP (unit: mm).

(model BK4371 from B&K) which was bonded to the other surface of CHSP and was back to back with the MPA (point A), and a Voltage Amplifier (Voltage AMP, model HVPA04 from XJTU).

The experimental way is also shown by Fig. 6, the excited signals are generated by PULSE system and output from the channel Output1 and then are transmitted directly to Power AMP. The amplified signals by Power AMP are transmitted to the electromagnetic shaker to excite the CHSP in point E. The measured signals from the acceleration transducer are amplified by the Charge AMP to transmit to the channel Input1 of PULSE system for recording and analysis. Synchronously, the measured acceleration signals are transmitted to the channel ADCH17 of dSPACE system as the original signals of the feedback controller. The control signals generated by the controller are output from the channel DACH1 of dSPACE system, and then they are applied in MPA after being amplified by Voltage AMP.

4.2. Experimental results

The experiments are classed as the resonant vibration control experiments and the sinusoidal swept experiments of the CHSP with vibration control. The resonant vibration control experiments include three cases as Case 1, Case 2 and Case 3 which are corresponding with the resonant excitation under the first three modal frequencies, respectively. The sinusoidal swept experiments just is measured the frequency response function curves of the CHSP with or without control.

In order to compare the effect of the number N of the PZT patch in MAP with the canceling result of the vibration of the CHSP, four experiments for the case of $N = 1$, 2, 3, 4 are performed in every cases. In experiments, for example $N = 1$, only the poles of the 1st layer PZT patch are applied the control voltage. At cases of $N = 2$, just only the poles of the 1st and 2nd layer PZT patches are applied the control voltage. The case of $N = 3$, 4 are also performed as the same way.

4.2.1. Delay time and feedback gain

Without doubt, the delay between the control signals and the response signals will limit the control effect of the actuators. Because the CHSP is a high damping structure and is controlled hard, in order to improve the control effect, the delay must be dealt with. In present experiment, we adopted the manual way to adjust the delay time in the dSPACE system by personal computer. Firstly, the delay times are confirmed in the three resonant control experiments only at the case of $N = 1$. When the amplitude of the acceleration response of the CHSP with control reach the lowest lever, the time value is confirmed as the delay time of the corresponding case. For the delay time to periodically appear, all the final confirmed delay times selected those that which are lower than the corresponding modal period. Moreover, in Case 1, Case 2 and Case 3, the delay times are same regardless of different number of the PZT patch, respectively. Finally the delay times D_1, D_2, and D_3 are confirmed as 10.6, 1.6 and 2.0 ms, respectively. Secondly, in order to control all the first three modes, the delay time D_0 in the sinusoidal swept experiments should close the value expressed as

$$D_0 \approx n_i T_i + D_i \quad (i = 1, 2, 3) \tag{18}$$

where n_i are integer, T_i, are the period of the ith mode. Note that, D_0 should be selected as less as possible. The delay time D_0 is confirmed as 12.352 ms finally.

The proportional velocity feedback control law is adopted in the present control experiments. In order to achieve the vibration cancellation, all the feedback gains are negative. Moreover, the same feedback gains are adopted at the case of Case 1, Case 2, Case 3 and at the sinusoidal swept experiments, respectively. In the present experiments, they are $G1 = -600$, $G2 = -780$ and $G3 = -500$ finally the resonant vibration control experiments. The gain $G0 = -1000$ is selected at the sinusoidal swept experiment.

4.2.2. Results of the resonant vibration control experiments

Fig. 7 shows the acceleration histories of the vibration of the uncontrolled and controlled CHSP at Case 1, Case 2 and Case 3. Moreover, the vibration control experiments are performed at the case of $N = 1$, 2, 3 and 4 in above three cases. Obviously, the acceleration responses of the CHSP are canceled with the starting of the feedback control, and the amplitude of the acceleration response is decreased with increasing of N in three cases after stability of the vibration control of the CHSP.

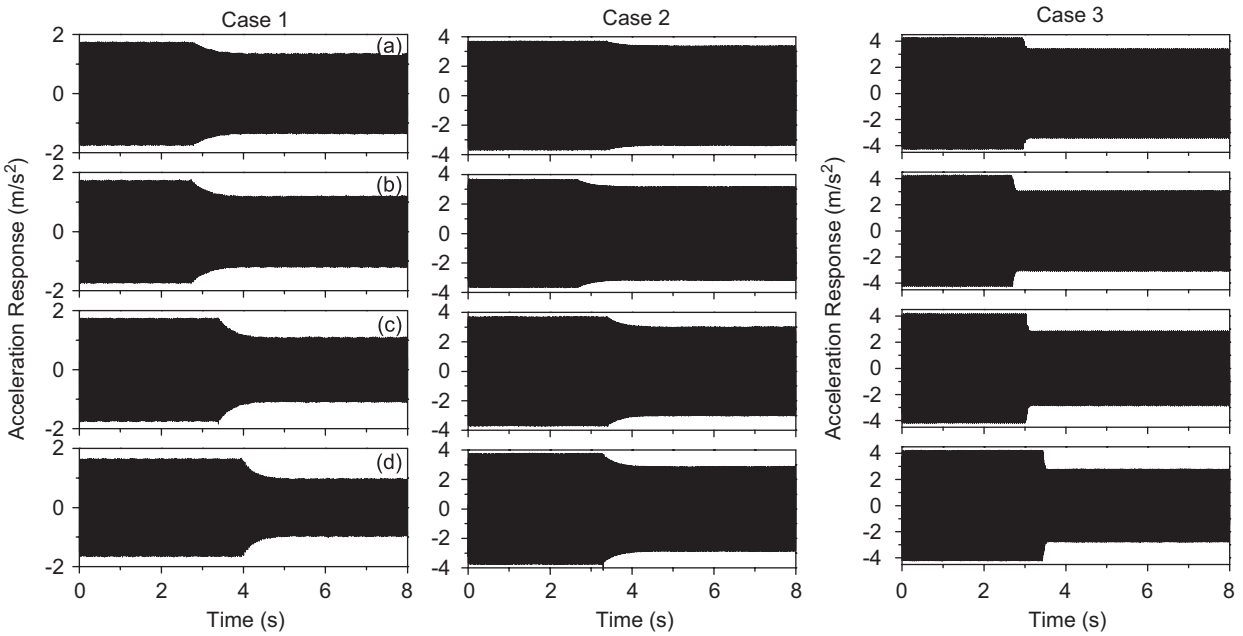

Fig. 7. Acceleration response for the case of Case 1, Case 2 and Case 3. (Number of PZT patch: (a) one layer; (b) two layers; (c) three layers; (d) four layers).

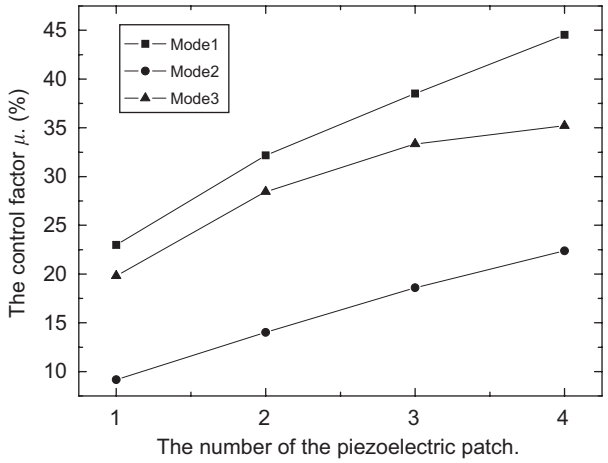

Fig. 8. The relations between the control factor μ and the number of the piezoelectric patch.

Furthermore, a control factor μ is defined as

$$\mu = \left| \frac{A_0 - A_c}{A_0} \right| \times 100\% \tag{19}$$

where A_c and A_0 are the acceleration amplitude of the CHSP with and without control, respectively. Fig. 8 shows the relations between the control factor μ and the number of the piezoelectric patch at the case of Case 1, Case 2 and Case 3.

On the other hand, the amplitudes of the control voltage are also decreasing with the increase of the number of the PZT patches. As shown in Fig. 9, the amplitudes of the control voltage observed by the Voltage AMP

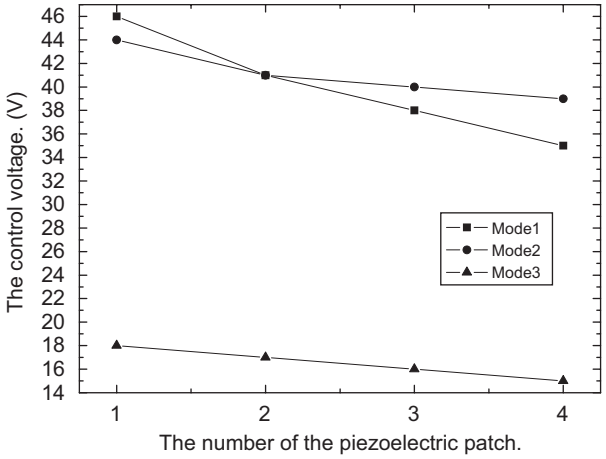

Fig. 9. The control voltage relates with the number of the piezoelectric patch.

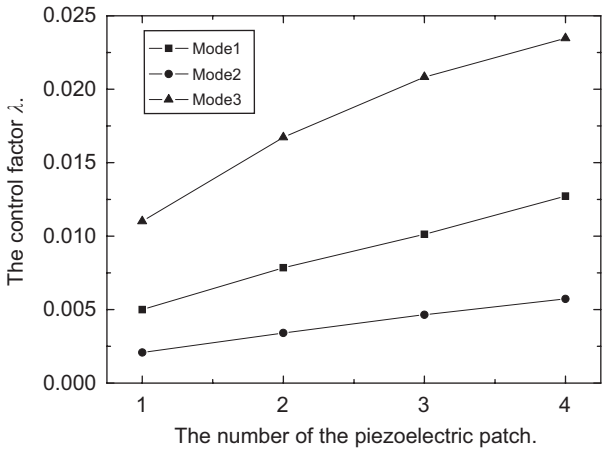

Fig. 10. The control factor λ relates with the number of the piezoelectric patch at the feedback point.

are ± 46 V ($N = 1$), ± 41 V ($N = 2$), ± 38 V ($N = 3$) and ± 35 V ($N = 4$) at the case of Case 1 after stability of the control system, respectively. The amplitudes of the control voltage are ± 44 V ($N = 1$), ± 41 V ($N = 2$), ± 40 V ($N = 3$) and ± 39 V ($N = 4$) at the case of Case 2 and are ± 18 V ($N = 1$), ± 17 V ($N = 2$), ± 16 V ($N = 3$) and ± 15 V ($N = 4$) at the case of Case 3, respectively. These results mean that the electrical source is only needed to provide a low level voltage if N is increased suitably. In order to compare the control effect of the MPA with different PZT layers under unit control voltage, the control factor λ is defined as

$$\lambda = \mu / V = \left| \frac{A_0 - A_c}{A_0 V} \right| \times 100\% \tag{20}$$

where V is the amplitude of control voltage. Fig. 10 shows the relations between the control factor λ and the number of the piezoelectric patch at three cases. It indicates that the control effect per unit control voltage is linearly increasing besides that of Case 3. The phenomena in Case 3 may indicate that the actuated capability of present actuator will be limited at certain high control lever.

4.2.3. Results of the sinusoidal swept experiments

Fig. 11(a) shows the frequency response function (FRF) curves of the CHSP with or without control which measured in the sinusoidal swept experiments. In order to observe the peak value of the FRF curves,

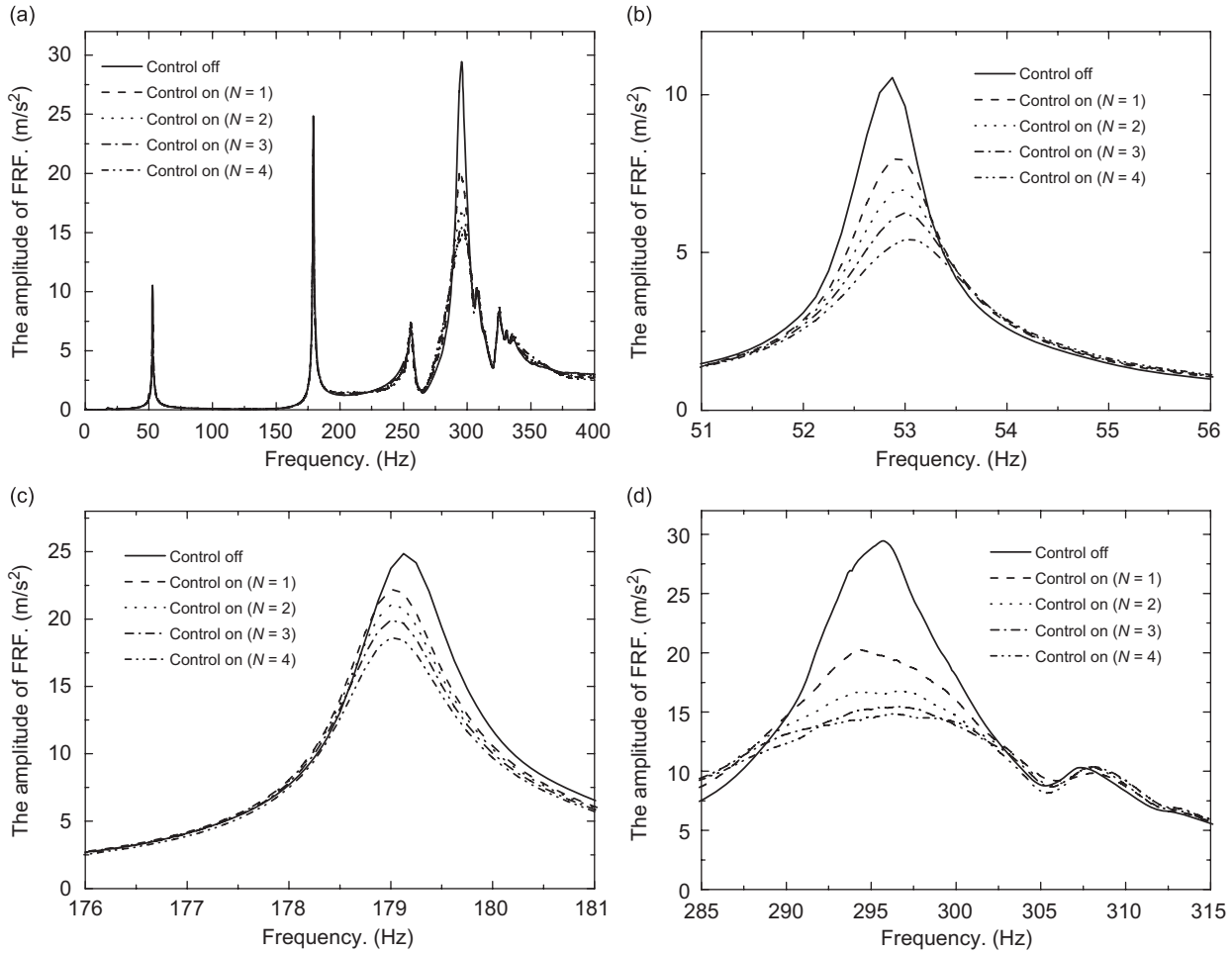

Fig. 11. The frequency response function curves.

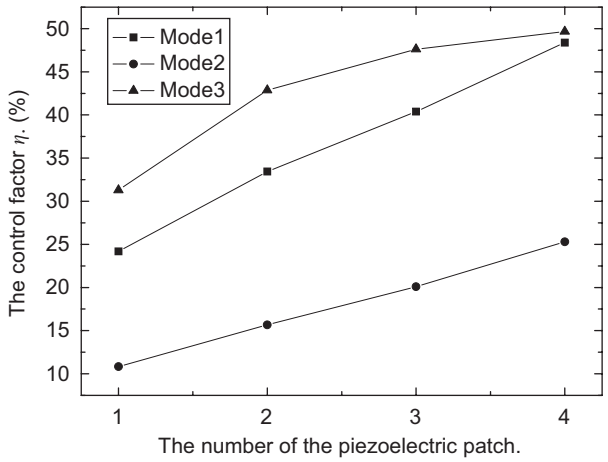

Fig. 12. The control factor η of the FRF relates with the number of the piezoelectric patch at the feedback point.

Fig. 11(b)–(d) give the local FRF curves around the first mode, second mode and third mode, respectively. It is found that the peak values are decreased with the increasing of the number of PZT patch in all modes. Similar to the resonant control experiments, the decreasing extent of the peak value is limited with the increasing of the number of PZT patch at the third mode. Furthermore, the control factor η is defined as

$$\eta = \left|\frac{P_0 - P_c}{P_0}\right| \times 100\% \tag{21}$$

where P_c and P_0 are the peak value of the FRF curves of the CHSP with and without control, respectively. The relations between the control η and N are shown in Fig. 12. It is found that the character of the relations is similar with that of Fig. 10.

5. Conclusions

A novel MPA is applied to vibration control of HSP in this paper. The electro-mechanical coupling equations of the system are derived using Hamilton principle. The formulas of actuation force and moment (over unit area per control voltage) of the actuator are also obtained, which show both actuation force and actuation moment are the four-order polynomial function of the number of used piezoelectric patches. However a numerical simulation indicated that the relations between actuation force/moments and the piezoelectric layers number are practically approximately linear. But the actuation capability is improved with the increase of the number of piezoelectric patches used.

In order to evaluate fully the actuation ability of the MPA, the active control experiment of a cantilever honeycomb sandwich panel is performed in this paper. The results show the MPA can restrain the vibration amplitude of the system which is under the resonant vibration from the resonant vibration control experiments, especially the first mode, with the maximum reduction of 44.54% for 4-layer actuator. And the MPA can suppress all three modes of the system in the examined frequency range from the sinusoidal swept experiments. Besides, as the number of piezoelectric patches used in the actuator increases, the control performance achieved by unit driven voltage is improved significantly. It implies that, under the same drive voltage, the MPA can attenuate the vibrations of CHSP more significantly than single piezoelectric patch actuator. Moreover, it is helpful that the control voltages applied in the MPA are decreased with the increase of the number of piezoelectric patches used. In this paper, some parameters of the MPA, for instance the displacement, size and so on, are not considered particularly though they are important to the effect of the vibration control. But we will report the study of these parameters in the application of the MPA in the structural shape control in the future.

Acknowledgments

This work was supported by the National Natural Science Foundation of China under Grant no. 50275114.

Appendix A. Generalized internal force components

$$\begin{aligned}
\mathbf{M}_x^i &= F_z^i(\sigma_x^i z) = A_1^i\varphi_{x,x} + A_2^i\varphi_{y,y} + A_3^i w_{,xx} + A_4^i w_{,yy} + A_5^i e_{31}E_3\\
\mathbf{M}_y^i &= F_z^i(\sigma_y^p z) = B_1^i\varphi_{x,x} + B_2^i\varphi_{y,y} + B_3^i w_{,xx} + B_4^i w_{,yy} + B_5^i e_{32}E_3\\
\mathbf{M}_{xy}^i &= F_z^i(\tau_{xy}^p z) = C_1^i\varphi_{x,y} + C_2^i\varphi_{y,x} + C_3^i w_{,xy}\\
\mathbf{R}_x^i &= \frac{1}{3(h+d+HN(t_p+t_v))^2}F_z^i(\sigma_x^p z^3) = D_1^i\varphi_{x,x} + D_2^i\varphi_{y,y} + D_3^i w_{,xx} + D_4^i w_{,yy} + D_5^i e_{31}E_3\\
\mathbf{R}_y^i &= \frac{1}{3(h+d+HN(t_p+t_v))^2}F_z^i(\sigma_y^p z^3) = E_1^i\varphi_{x,x} + E_2^i\varphi_{y,y} + E_3^i w_{,xx} + E_4^i w_{,yy} + E_5^i e_{32}E_3
\end{aligned}$$

$$\mathbf{R}^i_{xy} = \frac{1}{3(h+d+HN(t_p+t_v))^2} F^i_z(\tau^p_{xy} z^3) = F^i_1 \varphi_{x,y} + F^i_2 \varphi_{y,x} + F^i_3 w_{,xy}$$
$$\mathbf{Q}^i_{xz} = F^i_z(\tau^p_{xz}) = a^i(\varphi_x + w_{,x})$$
$$\mathbf{Q}^i_{yz} = F^i_z(\tau^p_{yz}) = b^i(\varphi_y + w_{,y})$$
$$\mathbf{T}^i_{xz} = \frac{1}{(h+d+HN(t_p+t_v))^2} F^i_z(\tau^p_{xz} z^2) = c^i(\varphi_x + w_{,x})$$
$$\mathbf{T}^i_{yz} = \frac{1}{(h+d+HN(t_p+t_v))^2} F^i_z(\tau^p_{yz} z^2) = d^i(\varphi_y + w_{,y})$$

where the superscript i represents the faceplate of HSP ($i=f$), the honeycomb core ($i=c$), the piezoelectric patches ($i=p$) and the adhesive layers ($i=v$). Note that the coefficients A^i_5, B^i_5, D^i_5 and E^i_5 are nonzero only for $i=p$. The function $F^i_z(\bullet)$ denotes the integration (and summation) operation as followed:

$$F^f_z(\bullet) = \int_{-h-d}^{-h} (\bullet)\mathrm{d}z + \int_{h}^{h+d} (\bullet)\mathrm{d}z$$
$$F^c_z(\bullet) = \int_{-h}^{h} (\bullet)\mathrm{d}z$$
$$F^p_z(\bullet) = \sum_{j=1}^{N} \int_{h+d+jt_v+jt_p}^{h+d+jt_v+jt_p} (\bullet)\mathrm{d}z$$
$$F^v_z(\bullet) = \sum_{j=1}^{N} \int_{h+d+(j-1)t_v+(j-1)t_p}^{h+d+jt_v+(j-1)t_p} (\bullet)\mathrm{d}z$$

Here, for simplicity, define the following coefficients:

$$A^h_j = A^f_j + A^c_j, \quad j=1,\ldots,4 \qquad C^h_j = C^f_j + C^c_j, \quad j=1,\ldots,3 \qquad E^h_j = E^f_j + E^c_j, \quad j=1,\ldots,4$$
$$A^m_j = A^p_j + A^v_j, \quad j=1,\ldots,5 \qquad C^m_j = C^p_j + C^v_j, \quad j=1,\ldots,3 \qquad E^m_j = E^p_j + E^v_j, \quad j=1,\ldots,5$$
$$B^h_j == B^f_j + B^c_j, \quad j=1,\ldots,4 \qquad D^h_j = D^f_j + D^c_j, \quad j=1,\ldots,4 \qquad F^h_j = F^f_j + F^c_j, \quad j=1,\ldots,3$$
$$B^m_j = B^p_j + B^v_j, \quad j=1,\ldots,5 \qquad D^m_j = D^p_j + D^v_j, \quad j=1,\ldots,5 \qquad F^m_j = F^p_j + F^v_j, \quad j=1,\ldots,3$$

and

$$K^k_1 = A^k_1 - D^k_1, \qquad L^k_1 = C^k_1 + B^k_1 - E^k_1 - F^k_1,$$
$$K^k_2 = C^k_1 - F^k_1, \qquad L^k_2 = C^k_2 - F^k_2,$$
$$K^k_3 = A^k_2 + C^k_2 - D^k_2 - F^k_2, \qquad L^k_3 = C^k_3 + B^k_3 - E^k_3 - F^k_3,$$
$$K^k_4 = A^k_3 - D^k_3, \qquad L^k_4 = B^k_2 - E^k_2,$$
$$K^k_5 = A^k_4 + C^k_3 - D^k_4 - F^k_3, \qquad L^k_5 = B^k_4 - E^k_4,$$
$$K^h_6 = -(a^f + a^c + a^p + a^v), \qquad L^h_6 = -(b^f + b^c + b^p + b^v),$$

$$P^k_1 = D^k_1,\ P^k_2 = E^k_2,\ P^k_3 = D^k_2 + 2F^k_2,\ P^k_4 = E^k_1 + 2F^k_1,\ P^k_5 = D^k_3,\ P^k_6 = D^k_4 + E^k_3 + 2F^k_3,\ P^k_7 = E^k_4$$
$$P^h_8 = (a^f + a^c + a^p + a^v - c^f - c^c - c^p - c^v),\ P^h_9 = (b^f + b^c + b^p + b^v - d^f - d^c - d^p - d^v),$$

where the superscript k represents the HSP ($k=h$) and the MPA ($k=m$).

Appendix B. The general boundary conditions in explicit form of the laminated structure

$$\{[(A_1^i - D_1^i)\varphi_{x,x} + \frac{1}{2}(A_2^i + B_1^i - D_2^i - E_1^i)\varphi_{y,y} + \frac{1}{2}(A_3^i - D_1^i - D_3^i)w_{,xx} + \frac{1}{2}(A_4^i - D_4^i - E_1^i)w_{,yy}] - (\mathbf{M}_x^{bc} - \mathbf{R}_x^{bc})\}\delta\varphi_x = 0,$$

$$\{[(C_2^i - F_2^i)\varphi_{y,x} + \frac{1}{2}(C_1^i + C_2^i - F_2^i - F_1^i)\varphi_{x,y} + \frac{1}{2}(C_3^i - 2F_2^i - F_3^i)w_{,xy}] - (\mathbf{M}_{xy}^{bc} - \mathbf{R}_{xy}^{bc})\}\delta\varphi_y = 0,$$

$$\{[-D_3^i w_{,xx} + \frac{1}{2}(A_3^i - D_1^i - D_3^i)\varphi_{x,x} + \frac{1}{2}(B_3^i - D_2^i - E_3^i)\varphi_{y,y} - \frac{1}{2}(D_4^i + E_3^i)w_{,yy}] + \mathbf{R}_x^{bc}\}\delta w_{,x} = 0,$$

$$\{[-F_3^i w_{,xy} + \frac{1}{2}(C_3^i - 2F_2^i - F_3^i)\varphi_{y,x}] + \mathbf{R}_{xy}^{bc}\}\delta w_{,y} = 0,$$

$$\{[D_3^i w_{,xxx} + F_3^i w_{,xyy} - \frac{1}{2}(A_3^i - D_1^i - D_3^i)\varphi_{x,xx} - \frac{1}{2}(B_3^i - D_2^i - E_3^i)\varphi_{y,xy} - \frac{1}{2}(C_3^i - 2F_1^i - F_3^i)\varphi_{x,yy} + \frac{1}{2}(D_4^i + E_3^i)w_{,xyy} + (a^i - c^i)\varphi_x + (a^i - c^i)w_{,x}] - \mathbf{Q}_{xz}^{bc})\}\delta w = 0,$$

where $x = 0$ and $x = a$.

$$\{[(B_2^i - E_2^i)\varphi_{y,y} + \frac{1}{2}(A_2^i + B_1^i - D_2^i - E_1^i)\varphi_{x,x} + \frac{1}{2}(B_3^i - D_2^i - E_3^i)w_{,xx} + \frac{1}{2}(B_4^i - E_2^i - E_4^i)w_{,yy}] - (\mathbf{M}_y^{bc} - \mathbf{R}_y^{bc})\}\delta\varphi_y = 0,$$

$$\{[(C_1^i - F_1^i)\varphi_{x,y} + \frac{1}{2}(C_1^i + C_2^i - F_1^i - F_2^i)\varphi_{y,x} + \frac{1}{2}(C_3^i - 2F_1^i - F_3^i)w_{,xy}] - (\mathbf{M}_{xy}^{bc} - \mathbf{R}_{xy}^{bc})\}\delta\varphi_x = 0,$$

$$\{[-E_4^i w_{,yy} + \frac{1}{2}(A_4^i - D_4^i - E_1^i)\varphi_{x,x} + \frac{1}{2}(B_4^i - E_2^i - E_4^i)\varphi_{y,y} - \frac{1}{2}(D_4^i + E_3^i)w_{,xx}] + \mathbf{R}_y^{bc}\}\delta w_{,y} = 0,$$

$$\{[-F_3^i w_{,xy} + \frac{1}{2}(C_3^i - 2F_1^i - F_3^i)\varphi_{x,y}] + \mathbf{R}_{xy}^{bc}\}\delta w_{,x} = 0,$$

$$\{[E_4^i w_{,yyy} + F_3^i w_{,xxy} - \frac{1}{2}(B_4^i - E_2^i - E_4^i)\varphi_{y,yy} - \frac{1}{2}(A_4^i - D_4^i - E_1^i)\varphi_{x,xy} - \frac{1}{2}(C_3^i - 2F_2^i - F_3^i)\varphi_{y,xx} + \frac{1}{2}(D_4^i + E_3^i)w_{,xxy} + (b^i - d^i)\varphi_y + (b^i - d^i)w_{,y}] - \mathbf{Q}_{yz}^{bc})\}\delta w = 0,$$

where $y = 0$ and $y = a$.

References

[1] S.L. Venneri, B.K. Wada, M.C. Lou, Integrated utility module for NASA miniature spacecraft, IFA, 95-I, 401.

[2] Yajun Luo, Hongpang Niu, Weixiu Xu, Zhiguang Yang, Xinong Zhang, Dynamic characteristics and active control experiment of honeycomb plates, *Chinese Journal of Applied Mechanics* 23 (2) (2006) 267–270 (in Chinese).

[3] B. Petitjean, I. Legrain, F. Simon, S. Pauzin, Active control experiments for acoustic radiation reduction of a sandwich panel: feedback and feedforward investigations, *Journal of Sound and Vibration* 252 (1) (2002) 19–36.

[4] J.N. Reddy, On laminated composite plates with integrated sensors and actuators, *Engineering Structures* 21 (1999) 568–593.

[5] Giovanni Caruso, Sergio Galeani, Laura Menini, Active vibration control of an elastic plate using multiple piezoelectric sensors and actuators, *Simulation Modelling Practice and Theory* 11 (2003) 403–419.

[6] J.M.S. Moita, I.F.P. Correia, C.M. Mota Soares, C.A. Mota Soares, Active control of adaptive laminated structures with bonded piezoelectric sensors and actuators, *Computers and Structures* 82 (2004) 1349–1358.

[7] Zhang Xinong, Xie Shilin, Li Junbao, Zhang Jinghui, Experimental study of the controllable constrained damping layer structure with book model actuator, *Journal of Xi'an Jongtong University* 10 (1999) (in Chinese).

[8] A. Joshi, Multi-layered piezoelectric inserts as vibration control actuators, *Journal of Sound and Vibration* 253 (4) (2002) 917–925.

[9] V.G. Senthil, V.V. Varadan, V.K. Varadan, A review and critique of theories for piezoelectric laminates, *Smart Materials and Structures* 9 (1999) 24–28.

[10] A. Benjeddou, J. -F. Deü, S. Letombe, Free vibration of simply-supported piezoelectric adaptive plates: an exact sandwich formulation, *Thin-Walled Structures* 40 (2002) 573–593.

[11] I.F. Pinto Correia, et al., Active control of axisymmetric shells with piezoelectric layers: a mixed laminated theory with high order displacement field, *Computers and Structures* 80 (2002) 2265–2275.

[12] Ziya Koray Kusculuoglu, T.J. Royston, Finite element formulation for composite plates with piezoceramic layers for optimal vibration control applications, *Smart Materials and Structures* 14 (2005) 1139–1153.
[13] Moita, et al., Active control of adaptive laminated structures with bonded piezoelectric sensors and actuators, *Computers and Structures* 82 (2004) 1349–1358.
[14] Erasmo Carrera, A refined multilayered finite-element model applied to linear and non-linear analysis of sandwich plates, *Composites Science and Technology* 58 (1998) 1553–1569.
[15] D. Ballhause, M. D'Ottavio, B. Kroplin, E. Carrera, A unified formulation to assess multilayered theories for piezoelectric plates, *Computers and Structures* 83 (2005) 1217–1235.
[16] S.D. Yu, W.L. Cleghorn, Free flexural vibration analysis of symmetric honeycomb panels, *Journal of Sound and Vibration* 284 (2005) 189–204.
[17] J.N. Reddy, A simple higher-order theory for laminated composite plates, *Journal of Applied Mechanics* 51 (4) (1984) 745–752.
[18] T. Bailey, J.E. Hubbard, Distributed piezoelectric polymer active vibration control of a cantilever beam, *Journal of Guidance, Control, and Dynamics* 4 (1985) 595–609.
[19] D.E. Crawly, J. Luis, Use of piezoelectric actuators as elements of intelligent structure, *AIAA Journal* 25 (10) (1987) 1373–1385.
[20] W. Gawronski, Actuator and sensor placement for structural testing and control, *Journal of Sound and Vibration* 208 (1) (1997) 101–109.
[21] P. Liu, V.S. Rao, M. Derriso, Active control of smart structures with optimal actuator and sensor locations, *Proceedings of SPIE* 4693 (2002) 1–12.
[22] Z. Qiu, X. Zhang, H. Wu, H. Zhang, Optimal placement and active vibration control for piezoelectric smart flexible cantilever plate, *Journal of Sound and Vibration* 301 (2007) 521–543.
[23] Ayech Benjeddou, Jean-François Deü, A two-dimensional closed-form solution for the free-vibration analysis of piezoelectric sandwich plates, *International Journal of Solids and Structures* 39 (2002) 1463–1486.